Cement & Concrete Composites 31 (2009) 744–753

Contents lists available at ScienceDirect

Cement & Concrete Composites

journal homepage: www.elsevier.com/locate/cemconcomp

Water permeability of engineered cementitious composites

Michael D. Lepech [a,*], Victor C. Li [b]

[a] Department of Civil and Environmental Engineering, Stanford University, United States
[b] Department of Civil and Environmental Engineering, University of Michigan, United States

ARTICLE INFO

Article history:
Received 31 January 2008
Received in revised form 18 July 2009
Accepted 23 July 2009
Available online 28 July 2009

Keywords:
Engineered cementitious composites
ECC
Strain-hardening
Permeability
Self-healing
Durability

ABSTRACT

The water permeability of a unique class of high performance fiber reinforced cementitious composites (HPFRCC) called engineered cementitious composites (ECC) is investigated. These composites are deliberately tailored using microcmechanical design principles to exhibit pseudo-strain-hardening characteristics in uniaxial tension, up to greater than 4% strain. While undergoing tensile deformation, microcracks are designed to saturate the specimen rather than localize into large cracks. This tendency to form microcracks, which are experimentally shown to be approximately 60 μm in width, allows ECC material in the cracked state to maintain water permeability similar to that of uncracked concrete or mortar, and magnitudes lower than cracked reinforced mortar or concrete. It is also shown that the self-healing properties of cracks within ECC material significantly aids in reducing the coefficient of permeability of cracked ECC.

1. Introduction

A lack of durability is one of the most serious issues facing reinforced concrete construction subjected to harsh environmental conditions. One of the most severe concerns is the drastic decrease of durability associated with concrete cracking. It is well known that the durability of concrete structures in harsh environments is highly dependent upon the transport properties of the concrete material itself [1–3], therefore the various transport mechanisms of fluids within concrete have been the focus of many previous studies. Significant work has been done with regard to the transport mechanisms of permeability, absorption, and diffusion within hardened concrete. While many of these studies have examined uncracked concrete members [4–6], cracks undoubtedly form under both environmental and mechanical loads while in service. Once cracked, the transport properties of concrete materials change drastically [7–10]. A complete understanding of fluid transport within concrete materials, both cracked and uncracked, is critical to the development of durable reinforced concrete infrastructures.

The durability of reinforced concrete is typically associated with a minimization of both concrete degradation and reinforcing steel deterioration. The degradation of concrete can occur through such mechanisms as freeze thaw cycles, alkali–silicate reaction (ASR), fatigue stress, or sulfate reaction [11]. Steel deterioration is typically the result of either chloride penetration or carbonation of the concrete cover resulting in depassivation of the protective layer covering the steel reinforcement and leading to the oxidation of the reinforcing steel [12,13]. Worldwide, corrosion of reinforcing steel has been identified as the most prevalent and damaging form of deterioration in reinforced concrete structures [14]. Due to this, the reduction of chloride transport is vital to improving concrete durability.

Chloride transport can occur chiefly through three mechanisms; permeation, absorption, or diffusion. Respectively, these three mechanisms are driven by hydrostatic head, capillary action, or ion concentration gradient, all of which rarely occur simultaneously. Therefore, the prevalent transport mechanism for any individual structure is highly dependent on environmental surroundings. For permeation, a constant hydrostatic head is required, making this the transport mechanism most applicable to deep underwater or water retaining structures.

As mentioned, numerous studies have examined the permeability of both cracked and uncracked concrete. The permeability of uncracked concrete has been related principally to the particle density of the composite, typically a function of water to cement ratio. As particle density increases, there are fewer pores allowing for the flow of fluids through the matrix. Powers et al. [15] found that as the water to cement ratio decreases, water permeability decreases. This relation of low permeability to high density is one reason that high strength concretes, with significantly higher particle packing than normal concretes, are considered highly durable. However, high strength concretes, in comparison to normal strength concretes, show much higher levels of thermal shrinkage [16] and autogenous shrinkage [17]. Together with a high Young's

* Corresponding author. Tel.: +1 650 724 9459; fax: +1 650 723 7514.
E-mail address: mlepech@stanford.edu (M.D. Lepech).

0958-9465/$ - see front matter © 2009 Elsevier Ltd. All rights reserved.
doi:10.1016/j.cemconcomp.2009.07.002

modulus, low creep coefficient, and higher brittleness, these high strength concretes are far more likely than normal strength concretes to crack at an early age, and produce larger crack widths [18]. Once cracked, the permeability of concretes, regardless of matrix density or compressive strength, increases remarkably. As crack width grows from 100 μm to 500 μm, the permeability of concrete material has been shown to increase up to seven orders of magnitude [19].

The addition of fibers can aid in maintaining a lower permeability within cracked concrete. Studies performed by Tsukamoto [20] found that permeability within cracked concrete composites is proportional to the laminar flow rate between two parallel plates, as shown in

$$q_R = \xi \cdot q_G \tag{1}$$

where q_R is the flow rate through a crack (between two rough walls), ξ is the flow rate coefficient dependent on the type and tortuosity of cracking, and q_G .ed slot. This laminar flow rate increases proportionally with the cube of the distance between the parallel plates (i.e. crack width).

Tsukamoto reported that the addition of fibers to concrete leads to a decrease in the flow rate coefficient, ξ, due to a reduction in cracking tendency and increased microcracking. The incorporation of fibers also produced lower crack widths in fiber reinforced concrete (FRC) compared to plain concrete. Similarly, Stang and Aarre [21] found that the addition of fibers to concrete leads to significantly lower crack widths than seen in either plain or conventionally reinforced concrete. The effect of these two phenomenon, a decrease in the flow rate coefficient along with a decrease in crack width, acting simultaneously as a result of the addition of fibers allow for the possibility to reduce the permeability of cracked concrete materials to a level similar to uncracked concrete.

Engineered cementitious composites (ECC) is a unique type of high performance fiber reinforced cementitious composite (HPFRCC) which features high tensile ductility with moderate fiber volume fraction, typically 2% by volume [22]. Of special interest is the capability of ECC material to deform to high tensile strains, commonly over 4%, while designed to maintain very tight crack widths. These cracks have experimentally been shown on the order of 60–80 μm [23]. This high performance is possible through the use of steady state crack models which provide quantitative links between mesostructural properties such as fiber bridging properties and matrix toughness, and composite mechanical behavior such as steady state cracking stress and maximum crack width. To accommodate large deformations, rather than forming a small number of cracks which widen with increasing load as seen in concrete or tension-softening FRC, ECC forms numerous microcracks which allow the material to undergo pseudo-strain-hardening. Once initial microcracks widen to the typical 60 μm width at roughly 1% composite straining, additional microcracks form to accommodate further deformation while maintaining this tight crack width. This phenomenon is shown in Fig. 1. Consequently, crack width in ECC material is more a result of matrix and fiber interaction rather than steel reinforcement ratio. This inherent maximum crack width can be seen as a material property, similar to compressive strength or elastic modulus, rather than a structural property, such as reinforcing ratio in reinforced concrete. This uncoupling of the transport properties of ECC material to the required structural performance in any application (i.e. not requiring heavy reinforcement for crack control when not necessary for load resistance), allows designers significantly greater flexibility in meeting design challenges.

Reinforced concrete design codes currently do not specify precise limits on transport properties, such as a maximum concrete permeability, or a maximum crack width under load. The American Association of State and Highway Transportation Officials (AASHTO) [24] design codes relies on the computation of a "Z" factor for which maximum limits are set depending on the type of environmental exposure. The limit imposed within the AASHTO code corresponds to a minimum reinforcement spacing resulting in a crack width limit of approximately 350 μm. Within the American Concrete Institute (ACI) structural concrete design code [25] a maximum crack width is no longer explicitly calculated, however previous versions of the design code have suggested a maximum crack width of 300 μm for outdoor exposure. As discussed previously, at these relatively wide crack widths, the permeability of concrete material is nearly five orders of magnitude greater than that of sound concrete. While these crack width limits are important in reducing the transport of water and corrosives into reinforced concrete, they are far larger than allowable to effectively block corrosives from rapidly deteriorating the reinforcing steel, and potentially the entire reinforced concrete structure. Through the use of ECC material, which exhibits inherently tight crack widths under large tensile deformations, there exists the possibility of designing ECC cover materials with lower permeability and reinforced ECC structures with higher durability.

In this work, using micromechanics-based design methods, the theoretical basis for tailoring materials for tight crack width and correspondingly low permeability is established. Mechanical tests are then carried out to verify the ability of these new materials to maintain tight crack widths under uniaxial tension load. Finally, experimental permeability tests are carried out to compare the performance of new materials with steel reinforced cementitious materials and establish a fundamental crack width versus permeability relationship for multiple cracking materials.

2. Material design methodology

The primary design focus behind the development of cementitious composites with low permeability in the cracked state lies behind work performed by Wang et al. [19], Aldea et al. [26], Lawler et al. [7], and Rapoport et al. [27]. Wang et al. [19] reported that as crack width increases from 100 μm to 500 μm, the permeability coefficient increases nearly seven magnitudes from 1.0×10^{-11} m/s to 1.0×10^{-4} m/s. However, for crack widths under 100 μm, the permeability coefficient remains nearly identical to that of sound concrete, suggesting that for crack widths below this threshold there is no significant increase in permeability after cracking. The development of cementitious materials with low permeability after cracking can be accomplished by designing for maximum crack widths below 100 μm, even after substantial deformation and crack formation.

The seemingly diametric objectives of holding maximum crack widths below 100 μm while still accommodating large deformations can only be accomplished through the formation of large numbers of microcracks, which functionally spread the deformation out over a large area. As mentioned earlier, ECC material can be tailored to develop numerous closely spaced microcracks in a strain-hardening response when subjected to tensile loading. This tailoring is rooted in micromechanical design principles which focus on each of the three phases within the composite; mortar matrix, fiber, and the interface between them.

The first priority when designing ECC material for low permeability is to ensure the formation of multiple cracks and strain-hardening behavior under load. This allows large deformations to be distributed over numerous cracks, each exhibiting a crack width below the 100 μm threshold discussed previous. The basis of multiple cracking and strain-hardening within ECC is the propagation of steady state cracks which were first characterized by Marshall and Cox [28], and extended to fiber reinforced cementitious composites by Li and Leung [29] and Lin et al. [30]. By forming steady state "flat cracks" which maintain a constant crack width while

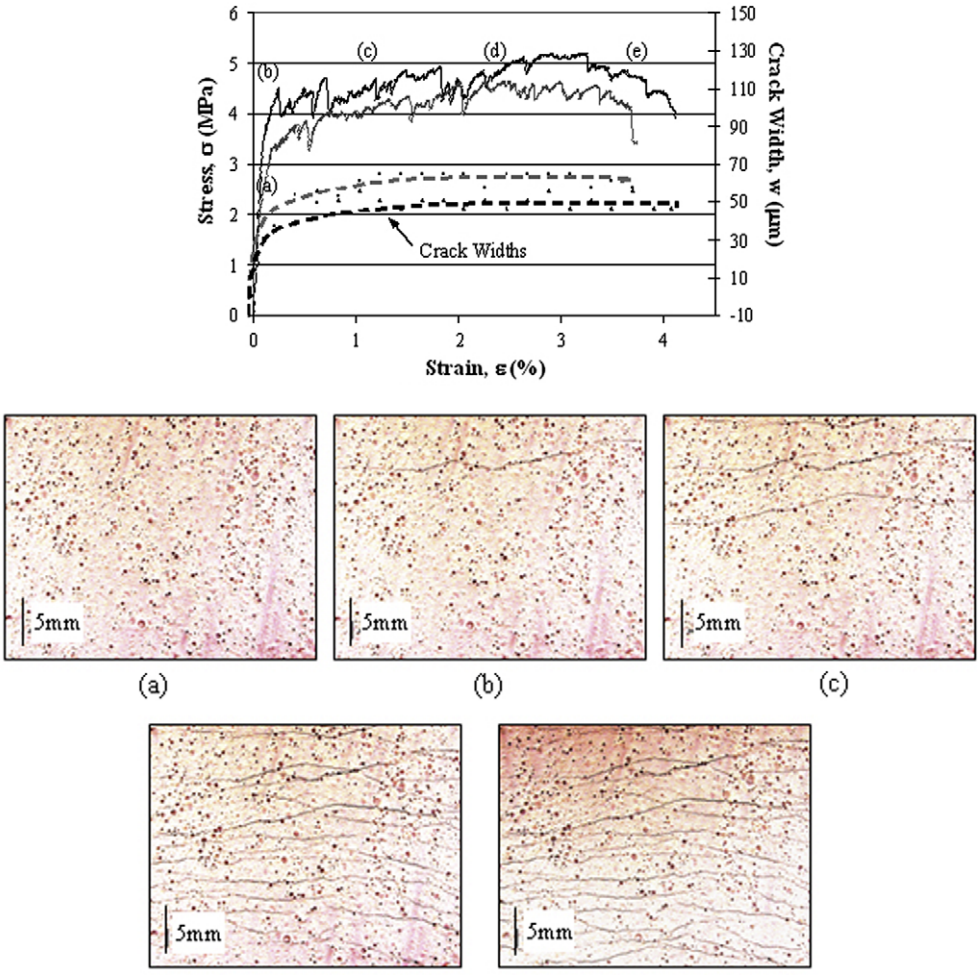

Fig. 1. Uniaxial stress strain curve and crack development of PVA–ECC M45.

propagating, rather than Griffith-type cracks which widen during propagation as in typical tension-softening fiber reinforced cementitious materials, ECC material exhibits multiple cracks with small widths which saturate the specimen while undergoing strain-hardening during extreme tensile deformation. The formation of multiple steady state cracking is governed by the bridging stress versus crack width opening relation along with the cracking toughness of the mortar matrix. To achieve this phenomenon the inequality shown in Eq. (2) must be satisfied.

$$J'_b = \sigma_0\delta_0 - \int_0^{\delta_0} \sigma(\delta)d\delta \geqslant J_{tip} \approx \frac{K_m^2}{E_m} \tag{2}$$

where J'_b is the complimentary energy shown in Fig. 2, σ_0 and δ_0 are the maximum crack bridging stress and corresponding crack opening, J_{tip} is the fracture energy of the mortar matrix crack tip, K_m is the fracture toughness of the mortar matrix, and E_m is the elastic modulus of the mortar matrix. In addition to the fracture energy criterion, a strength criterion expressed in Eq. (3) must be satisfied.

$$\sigma_0 > \sigma_{fc} \tag{3}$$

where σ_0 is the maximum crack bridging stress and σ_{fc} is the first cracking strength of the mortar matrix. For saturated multiple cracking, Wang and Li [31] found that Eq. (3) must be satisfied at each potential crack plane, where σ_{fc} is understood as the cracking stress on that crack plane.

Once an ECC mixture is selected which sufficiently meets the two above criteria, the formation of multiple steady state cracks,

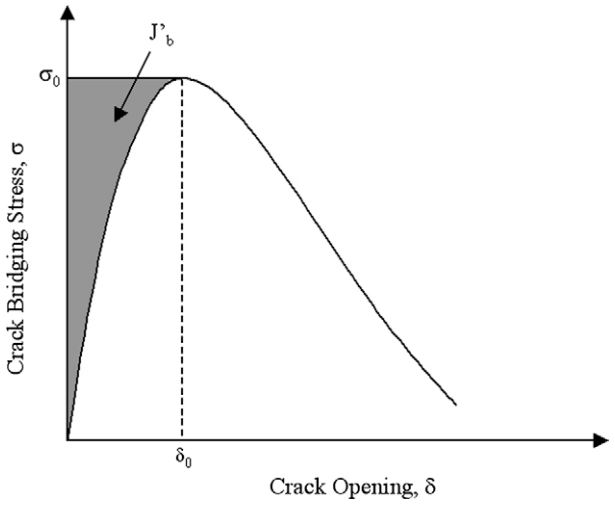

Fig. 2. Crack bridging stress versus crack opening relation.

and strain-hardening performance, can be realized. However, in addition to forming these cracks, the material must also be designed to exhibit crack widths below the 100 μm threshold limit. This can be achieved through tailoring of the crack bridging versus crack opening relation referenced in Eq. (2). Shown in Fig. 2, the maximum steady state crack width exhibited during ECC multiple

cracking is δ_0, the crack width corresponding to the maximum crack bridging stress, σ_0. If the crack width were to grow beyond δ_0, the crack bridging stress would begin to fall, in which case the crack would localize and multiple crack formation would cease. By keeping δ_0 below the 100 μm threshold, the ECC material can exhibit multiple cracking and strain-hardening performance, while maintaining crack widths small enough to limit permeability through the cracked material.

Lin et al. [30] proposed the formulation of the crack bridging stress versus opening relationship based on single fiber pullout performance. This relation in expressed in

$$\sigma(\delta) = \frac{4V_f}{\pi d_f^2} \int_{\phi=0}^{\pi/2} \left(\int_{z=0}^{(L_f/2)\cos\phi} P(\delta) e^{f\phi} p(\phi) p(z) dz \right) d\phi \quad (4)$$

where V_f is the fiber volume fraction, d_f is the fiber diameter, ϕ is the orientation angle of the fiber, L_f is the fiber length, z is the centroidal distance of a fiber from the crack plane, f is a snubbing coefficient, and $p(\phi)$ and $p(z)$ are probability density functions of the fiber orientation angle and centroidal distance from the crack plane, respectively. $P(\delta)$ is the pullout load versus displacement relation of a single fiber aligned normal to the crack plane, also described in Lin et al. [30].

Empirical properties in Eq. (4), such as the fiber snubbing coefficient, have been determined for ECC materials using a variety of fibers [32]. By varying fiber volume fraction, fiber diameter and length, fiber–matrix interface properties ($P(\delta)$ behavior), and fiber orientation (1D, 2D, or 3D), a theoretical composite can be designed to undergo large deformations, up to several percent, by generating large numbers of microcracks. By limiting the numerical value of δ_0 (the maximum value of $\sigma(\delta)$ from Eq. (4)) within the composite, maximum crack width is controlled and ductility is achieved without sacrificing low permeability due to crack growth and localization. Maximum crack width δ_0 is not exceeded in the composite as a result of the energy and strength multiple cracking constraints (Eqs. (2) and (3)) which ensure that before a crack in ECC reaches a width of δ_0, an adjacent microcrack will form and relieve the ambient stress level. The application of these material design procedures allow materials engineers to carefully match material characteristics to specific structural demands, such as strain capacity and low permeability. Using the theoretical constituent and composite properties determined from the $\sigma(\delta)$ response, actual mix proportions can be developed to fit theoretical requirements of fiber volume fraction, fiber–matrix interface properties, fiber orientation, etc.

3. Experimental procedure

Micromechanical experimental testing began on ECC material to verify that it meets both the conditions of strain-hardening performance, and maximum crack widths below 100 μm. Testing was done on an ECC mix designs designated Mix 45. The mix proportions for this version of ECC are shown in Table 1. The components of ECC material are similar to typical fiber reinforced cement composites (FRCC), consisting of Type I Portland cement, sand, class F fly ash, water, fibers, and a high range water reducing agent (HRWR). However, unlike typical FRCCs, the proportions within ECC are carefully determined through the use of the micromechanical design tools outlined above to achieve the desired strain-hardening response. To minimize the mortar matrix fracture toughness, no large aggregates are used, and the silica sand has an average and maximum grain size of 100 μm and 200 μm, respectively. The poly-vinyl-alcohol (PVA) fibers are purposely manufactured with a tensile strength, elastic modulus, and maximum elongation matching those needed for strain-hardening performance. Additionally, the surface of the PVA fibers is coated 1.2% by weight with a proprietary hydrophobic oiling agent to tailor the interfacial properties between fiber and matrix for strain-hardening performance [32]. Specific attributes of the PVA fibers used in this study are shown in Table 2.

In addition to ECC, the permeability of cracked and uncracked reinforced (with steel wire mesh) mortar specimens was also tested as a control test series. The mix proportions of the mortar specimens are also shown in Table 1. The components of this material are Type I Portland cement, water, and a standard Ottawa sand. To generate different crack widths and crack spacing among the mortar samples, the level of reinforcement within the specimens was varied. The reinforcement ratios of the mortar samples and their test designations is shown in Table 3. Mixing of all ECC and mortar materials within this study was done using a force-based Hobart mixer.

3.1. Test specimen preparation and test execution

For determination of micromechanical characteristics of the ECC fiber–matrix interface, particularly J_b' and the bridging stress versus crack opening relation, single strands of PVA fibers were pulled from the M45 matrix under displacement control. Single fiber pullout tests allow for the determination of the fiber pullout load versus pullout displacement curve, P–δ, used to compute the composite bridging stress versus crack opening relation. This testing follows procedures outlined by Redon et al. [33]. Single fiber pullout specimens were tested after 14 days of wet curing to correspond with the time at which the permeability specimens would be tested in uniaxial tension.

Determination of matrix cracking energy on ECC M45 matrices was performed using notched beams. Prisms of ECC matrix (identical to ECC material but without fibers) measuring 75 mm × 38 mm × 300 mm were cast and cured in air for 14 days. After curing, a 2 mm wide × 30 mm deep notch was cut at the midspan of each prism. Prisms were tested in bending to determine the load at failure (i.e. crack propagation load). The matrix toughness, K_m, was calculated using the appropriate geometric calibration factors.

Table 1
Mix proportions of Ecc M45 and standard mortar (kg/m^3).

Material	Cement	Aggregates	Fly ash	Water	HRWR[a]	Fiber
ECC M45	578	462	694	319	7.51	26
Mortar	614	1534	–	215	–	–

[a] High range water reducer.

Table 2
Mechanical properties of PVA fiber.

Nominal strength (MPa)	Apparent strength (MPa)	Diameter (μm)	Length (mm)	Elastic modulus (GPa)	Elongation (%)
1620	1092	39	12	42.8	6.0

Table 3
Reinforced mortar and ECC steel reinforcement ratios, observed crack widths, and observed crack spacing.

Specimen series	Reinforcement ratio	Crack width (μm)	Crack spacing (mm)
R/M[a]-a	0.019	350–500	20–30
R/M-b	0.023	200–350	10–25
R/M-c	0.028	125–200	5–15
ECC	0	40–80	2–5

[a] R/M denotes reinforced mortar specimen series.

To characterize permeability as a function of crack width for a wide range of crack widths in ECC and reinforced concrete materials, both ECC and reinforced mortar permeability testing specimens were cast. These were then loaded in uniaxial tension to produce multiple crack patterns of various widths for a constant specimen strain (elongation). ECC permeability specimens were cast into tensile testing plates with cross sectional dimensions of 12 mm × 75 mm. Tensile specimens measure 300 mm in length with a gauge length of 180 mm during testing. Tensile specimens were air cured for 14 days prior to uniaxial tension testing. The testing regime followed that proposed by Li et al. [32]. Following this testing, ECC specimens were kept in water for an additional 14 days to ensure complete water saturation prior to further testing. Cracks widths in all specimens were measured load at 30 individual locations after removing all on the specimen using an optical microscope with an internal crack width gauge. Permeability testing began at 28 days. A deformation limit was chosen a priori as an appropriate permeability test level for comparison with the control mortar specimens. An initial set of ECC specimens was prepared which was strained to a value of 1.5%. At 1.5% deformation, the reinforced mortar specimens (with reinforcing ratios ranging from 1.9% to 2.9%) had developed large cracks, and had failed in some cases. Details for both the reinforced mortar and ECC specimens are given in Table 3. For the second round of ECC permeability testing, separate ECC specimens were strained from 0% to 3%. Representative stress versus strain curves for the various ECC testing series can be found in Fig. 3.

Reinforced mortar specimens were cast into tensile plates with geometry identical to the ECC tensile plates. To generate differing crack widths and crack spacing among the specimens, various amounts of steel reinforcing mesh (ranging from 1.9% to 2.9%) was cast into the plates. All reinforced mortar specimens were deformed in uniaxial tension to 1.5% of the specimen gauge length. Reinforcement levels were varied a number of times until a representative group of specimens with a variety of crack widths and spacing was achieved, once again shown in Table 3.

3.2. Permeability testing

At an age of 28 days, the tensile specimen edges were sealed with epoxy to facilitate unidirectional flow through the cross section. Due to the length of time associated with this type of testing, crack width permeability measurements were performed in the unloaded state. To conduct permeability testing, two experimental setups were used. A falling head test was used for specimens with a low permeability, while a constant head test was used for specimens with a permeability too high to practically use the falling head test. These two setups are shown schematically in Fig. 4a and 4b, respectively. The falling head and constant head permeability test setups have been adapted from Wang et al. [19] and Cernica [34].

The permeability of specimens in the falling head test can be determined using Eq. (5), while the permeability of specimens in the constant head test can be determined using

$$k = \frac{a \cdot L}{A \cdot t_f}\left(\frac{h_0}{h_f}\right) \tag{5}$$

$$k = \frac{V \cdot L}{A \cdot h_0 \cdot t_f} \tag{6}$$

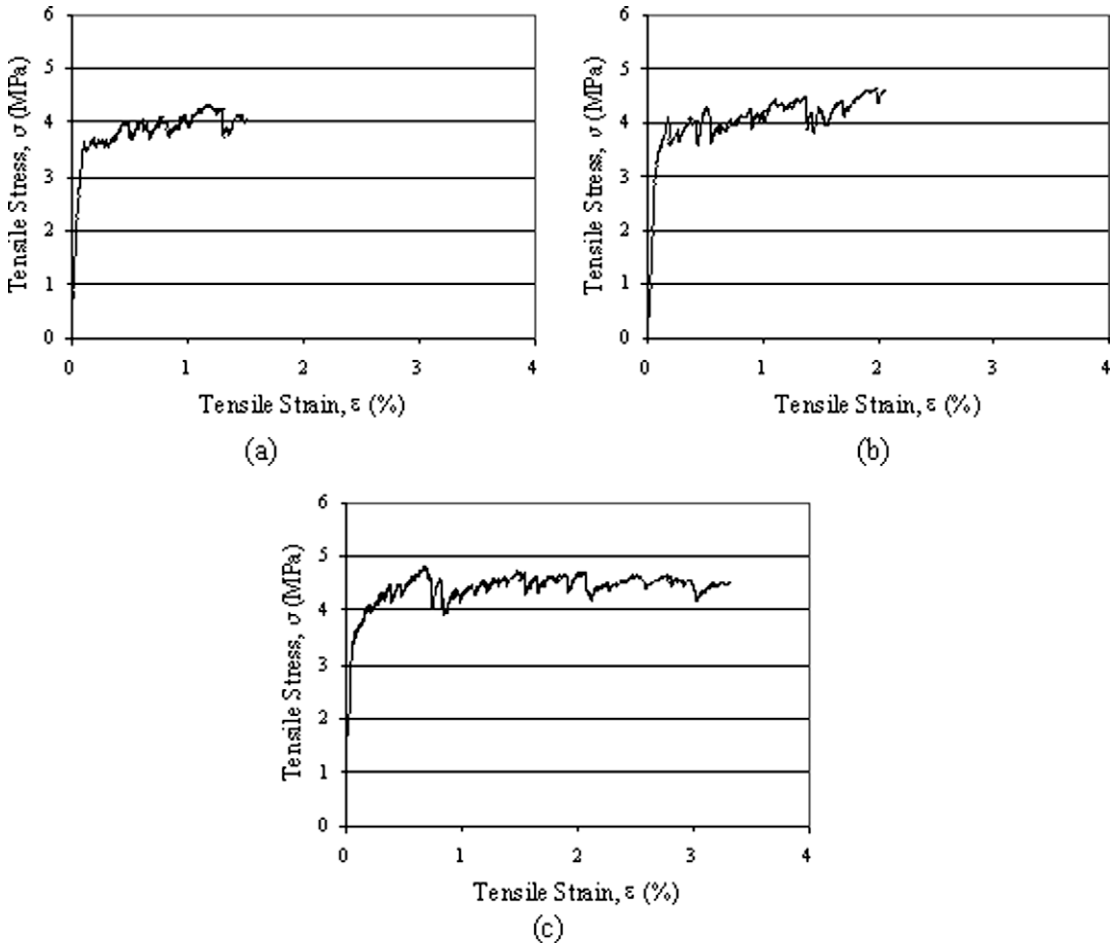

Fig. 3. Uniaxial tensile stress versus strain curves for ECC M45 deformed to: (a) 1.5%, (b) 2%, and (c) 3%.

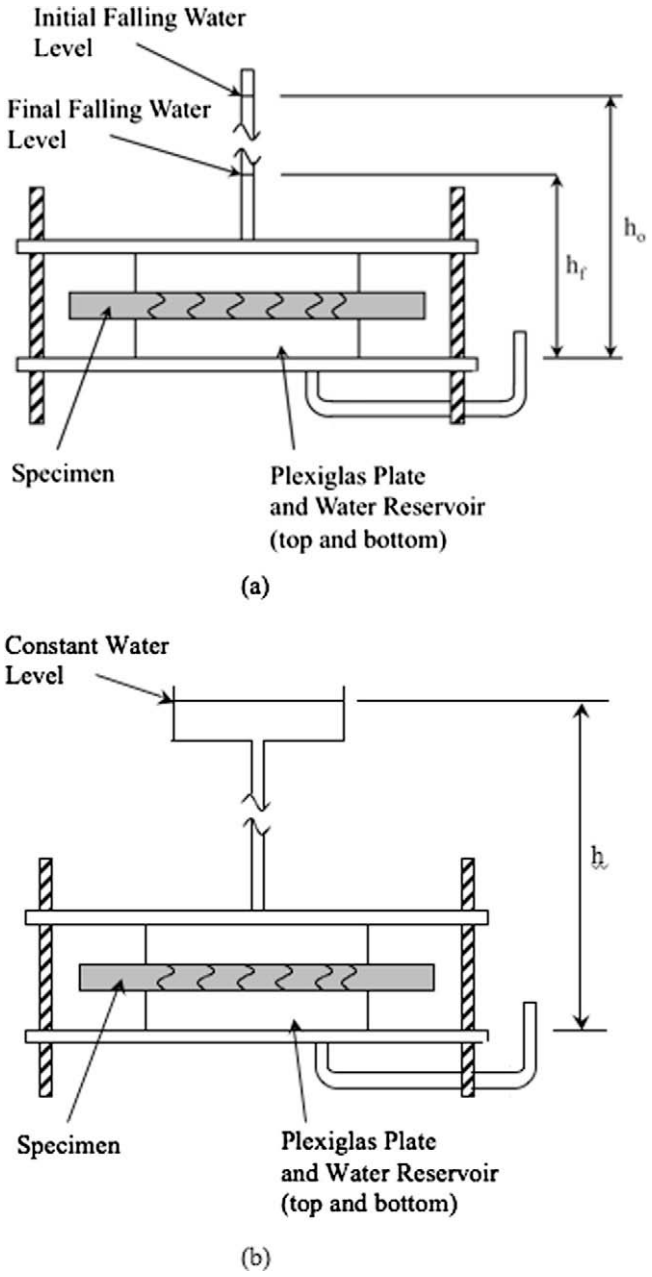

Fig. 4. (a) Falling head permeability test setup and (b) constant head permeability test setup.

where k is the coefficient of permeability, a is the cross sectional area of the standpipe, L is the specimen thickness in the direction of flow, A is the cross sectional area subject to flow, t_f is the test duration, h_0 is the initial hydraulic head, h_f is the final hydraulic head, and V is the volume of liquid passed through the specimen during the test. Geometric quantities used in these tests are given in Table 4.

However, Eq. (5) and Eq. (6) inherently assume homogeneous flow through the material by dividing the rate of flow by the experimental specimen cross sectional area. The use of very large specimens with a single crack can result in very low water permeability, regardless of the true rate of water permeation. Therefore, it is more appropriate to use Eqs. (5) or (6) on a cracked material such as ECC, which exhibits tightly spaced microcracks after large deformations creating a more homogeneous material, rather than reinforced or plain concrete or mortar even though both may be cracked. For comparison with results of other concrete materials research, the permeability coefficient for concrete or ECC should be normalized by the number of cracks within the specimen to produce a coefficient of permeability per crack, or normalized permeability, and thereby remove the influence of specimen cross sectional area.

Table 4
Geometric constants of permeability testing setup.

Quantity	a	L	A
Value	2.84×10^{-5} m^2	0.012 m	8.93×10^{-3} m^2

4. Experimental results and discussion

Results from testing of the micromechanical parameters suggest that the proposed ECC M45 mixes should exhibit strain-hardening characteristics, and maintain crack widths below the critical 100 μm threshold. The critical ratio of J_b'/J_{tip} lies above the value of unity, at approximately 1.08. While this ratio does not fall far above the strain-hardening cutoff, the current modeling of single fiber pullout (shown as Eq. (4)) does not take into account two-directional fiber pullout, or spalling of the matrix from pullout of angled fibers, both of which would serve to increase the complimentary energy of the composite. Therefore, this value of J_b'/J_{tip} for M45 is assumed to be a lower bound. As seen from Fig. 1, ECC M45 displays excellent strain-hardening characteristics, and the observed crack widths of ECC M45 range from 40 μm to 70 μm in the loaded state, well below the 100 μm limit outlined previously. When unloaded for permeability testing, ECC microcracks are observed to close approximately 10% of their loaded width (between 5 μm and 10 μm) and are reported as such for experimental permeability test results.

Overall findings for the water permeability comparison series between ECC and reinforced mortar samples are shown in Fig. 5 plotting maximum crack width in each material specimen versus the coefficient of permeability. These results are summarized in Table 5. As expected, the magnitude of permeability through the cracked reinforced mortar increases rapidly with an increase in crack width. For reinforced mortar specimens, water permeability ranges from 4.58×10^{-11} m/s for uncracked mortar specimens up to 4.46×10^{-4} m/s for crack widths of approximately 500 μm. This extreme variation, nearly seven orders of magnitude, has a profound impact on the overall performance of reinforced concrete in service. Historically, ACI [25] and AASHTO [24] design codes have recommended crack control reinforcement to limit crack widths under 300 μm and 350 μm, respectively. Yet even at this crack width, water permeability has increased six orders of magnitude, approximately 1.00×10^5 m/s.

Many concrete service life models (i.e. Life-365 [35]) assume that the concrete remains uncracked throughout the majority of service life, and once cracked it has little resistance to the penetration of water-borne corrosives resulting in rapid degradation. However, it is common for reinforced concrete to crack long before the end of service life due to free or restrained shrinkage stresses, thermal stresses, or simple overloading. The occurrence of any one of these phenomena during service life is practically guaranteed resulting in early age cracking, and premature ingress of corrosives. The durability of reinforced concrete is known to decrease drastically upon contact between corrosives and reinforcing steel. The wide cracks with large spacing in reinforced concrete have also been shown to form macro-cell corrosion potentials [36], resulting in severe pitting corrosion of the reinforcing steel and spalling of the concrete cover, undermining the basic assumptions within service life models.

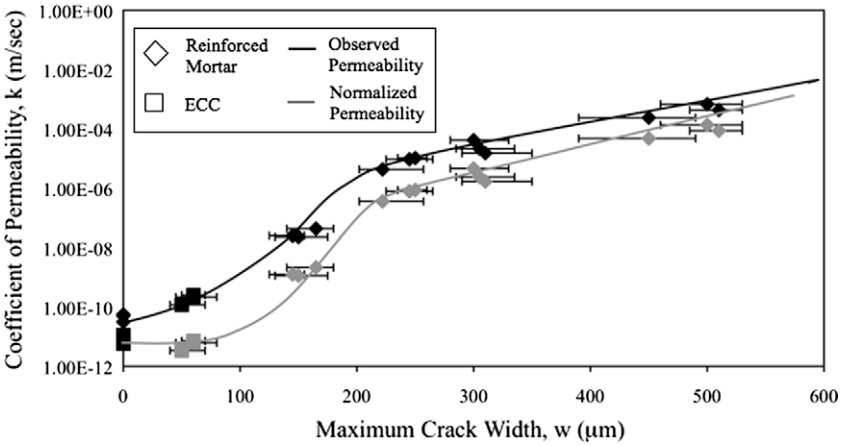

Fig. 5. Coefficient of permeability versus crack width for ECC and reinforced mortar series deformed to 1.5% in uniaxial tension.

Table 5
Water permeability of cracked and uncracked ECC and reinforced mortar specimens.

Series	Crack width (μm)	No. of cracks	Permeability (m/s)	Normalized permeability (m/s per crack)
R/M (uncracked)	0	0	$4.58 \times 10^{-11} \pm 1.2 \times 10^{-11}$	$4.58 \times 10^{-11} \pm 1.2 \times 10^{-11}$
R/M-a	150 ± 15	17	$3.02 \times 10^{-8} \pm 7.5 \times 10^{-9}$	$1.77 \times 10^{-9} \pm 4.4 \times 10^{-10}$
R/M-b	240 ± 18	11	$7.97 \times 10^{-6} \pm 2.3 \times 10^{-6}$	$7.24 \times 10^{-7} \pm 2.1 \times 10^{-7}$
R/M-b	300 ± 10	9	$2.58 \times 10^{-5} \pm 6.7 \times 10^{-6}$	$2.87 \times 10^{-6} \pm 7.4 \times 10^{-7}$
R/M-c	500 ± 50	5	$4.46 \times 10^{-4} \pm 4.2 \times 10^{-4}$	$8.92 \times 10^{-5} \pm 8.4 \times 10^{-5}$
ECC (uncracked)	0	0	$8.18 \times 10^{-12} \pm 2.4 \times 10^{-12}$	$8.18 \times 10^{-12} \pm 2.4 \times 10^{-12}$
ECC (1.5%)	50 ± 10	47	$1.95 \times 10^{-10} \pm 5.6 \times 10^{-11}$	$4.15 \times 10^{-12} \pm 1.2 \times 10^{-12}$
ECC (2%)	52 ± 10	59	$3.00 \times 10^{-10} \pm 6.8 \times 10^{-11}$	$5.08 \times 10^{-12} \pm 1.2 \times 10^{-12}$
ECC (3%)	63 ± 10	87	$7.74 \times 10^{-10} \pm 1.9 \times 10^{-10}$	$8.90 \times 10^{-12} \pm 2.2 \times 10^{-12}$

As designed, the ECC specimens subjected to 1.5% strain prior to testing exhibited a much lower coefficient of permeability due to the small crack widths. Cracks within the ECC specimens opened to a maximum width of approximately 60 μm. This resulted in a permeability coefficient of 1.95×10^{-10} m/s. This low permeability, nearly five orders of magnitude smaller than similarly strained mortar specimens with ACI or AASHTO recommended maximum crack widths, should serve to significantly improve the service-life performance of any structure constructed with ECC material which is exposed to water pressure.

While the results of ECC permeability measurements may seem to show an increase in permeability by one order of magnitude over the uncracked ECC and mortar, this result may be misleading. Cracked concrete permeability work performed by others [19,26,7,27], has been conducted primarily on specimens with a single crack. As mentioned previously Eqs. (5) and (6) inherently assume homogeneous flow through the material by dividing the rate of flow by the experimental specimen cross sectional area. For comparison with results of other researchers, the permeability coefficient are normalized by the number of cracks within the specimens to produce a coefficient of permeability per crack or normalized permeability. Once this is done, results between ECC material, with numerous 60 μm cracks, and concrete, with one 60 μm crack (1.00×10^{-11} m/s from Wang et al. [19]), match reasonably well.

The second series of ECC permeability specimens demonstrates that, in addition to exhibiting low permeability at relatively small strains (i.e. 1.5%), ECC material can exhibit low water permeability at higher levels of tensile strain. Regardless of the level of tensile deformation, ranging from 1.5% to 3.0%, water permeation through the cracked ECC specimens remained very low. This is shown graphically in Fig. 6. The water permeability of the ECC specimens strained to 2% and 3% uniaxial tension is 3.00×10^{-10} m/s and 7.74×10^{-10} m/s. Even as the number of cracks along the specimen grows, the permeability of the specimens does not change significantly, due to the inherently tight 60 μm crack widths maintained by the ECC material. This is evidenced by the crack saturation shown in Fig. 1. After normalizing by the number of cracks (from Table 5), the difference among ECC specimens strained to higher levels becomes even less significant. Once normalized by the number of cracks, the water permeability of ECC specimens strained to 2% and 3% uniaxial tension falls to 5.08×10^{-12} m/s and 8.90×10^{-12} m/s. This is also shown in Fig. 6.

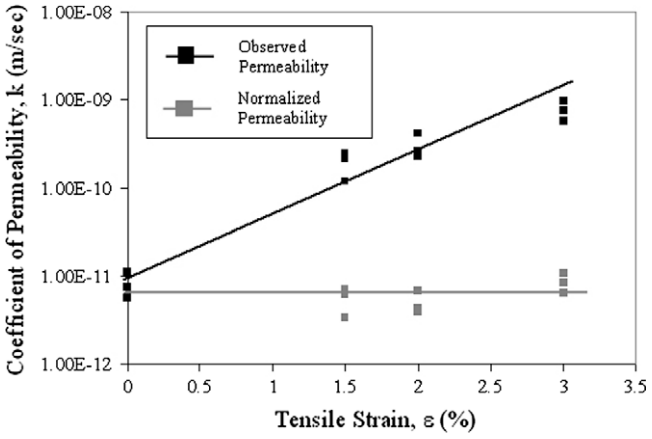

Fig. 6. Coefficient of permeability versus level of tensile strain in ECC.

Throughout the course of testing, it became apparent that the low crack widths exhibited among ECC specimens was not the only cause for the low water permeability of ECC specimens. As shown in Fig. 7, the rate of permeation through the ECC specimens

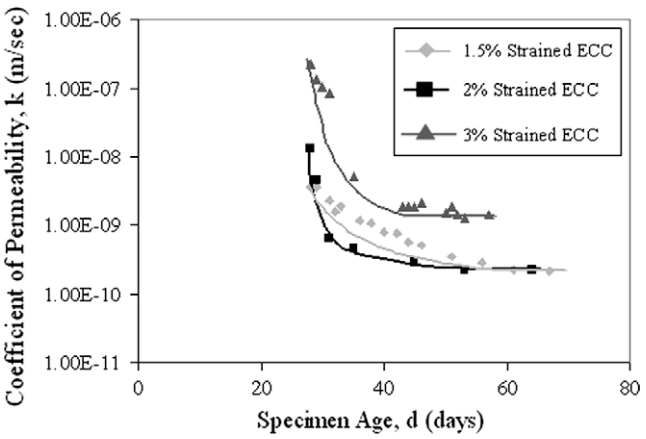

Fig. 7. Development of permeability for ECC strain to 1.5%, 2% and 3%.

dropped drastically from the initial values until asymptotically reaching the recorded value, even though the crack widths during permeability testing do not change. This phenomenon can be partially attributed to achieving complete saturation and further densification of the matrix throughout the testing period. However, ECC specimens were saturated in water for 14 days prior to permeability testing at an age of 28 days. By the time of testing, the specimens should have been nearly, if not completely, saturated and continuing to undergo little matrix hydration. Throughout the course of permeability testing, a white residue formed within the cracks and on the surface of the specimens near the cracks. These formations are shown in Fig. 8. Fig. 8a shows a saturated ECC specimen immediately prior to the beginning of permeability testing, while Fig. 8b shows the same specimen after permeability testing. The white residue forms both within the cracks, and within the pores on the surface of the ECC specimen. Fig. 8c and d show a cracked reinforced mortar specimen before and after permeability testing, respectively.

The effect of self-healing of cracks on permeability has been investigated by other researchers [37], and may be significant in the permeability determination of cracked ECC. This can be attributed primarily to the large binder content and relatively low water to binder ratio within the ECC mixture. The presence of significant amounts of unhydrated binders allows for autogeneous healing of the cracks when exposed to water. This mechanism is particularly evident in cracked ECC material due to the small crack widths which facilitate self-healing [37]. However, this phenomenon is not observed while cracked ECC specimens are simply saturated

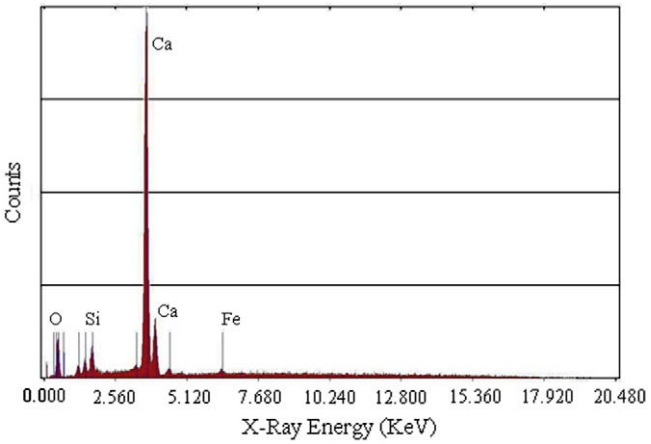

Fig. 9. ESEM surface chemical composition analysis of self-healing crack formations.

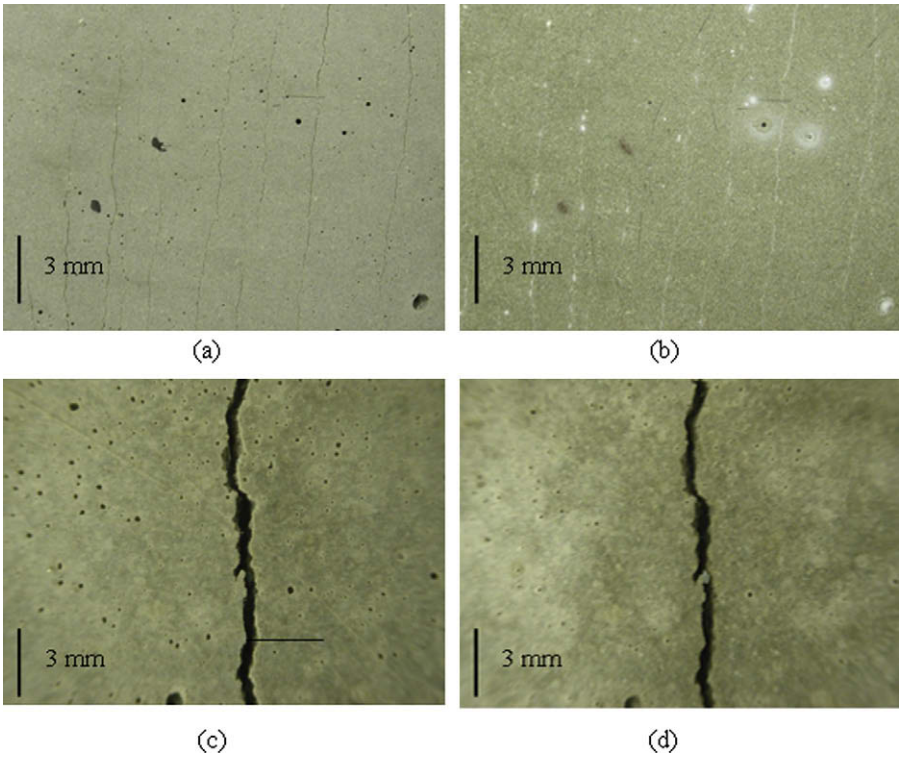

Fig. 8. Appearance of ECC permeability specimens: (a) before permeability testing and (b) after permeability testing and reinforced mortar specimens; (c) before permeability testing and (d) after permeability testing.

in water. During the 14 days of saturation prior to permeability testing, cracked ECC specimens showed no signs of autogeneous healing of the cracks. After only 3 days in the permeability testing apparatus, evidence of self-healing became apparent. A similar phenomenon was also seen when cracked ECC specimens were partially submerged in water. Crack healing was only exhibited near the surface of the water, while no healing was observed outside of this near-surface region.

Surface chemical analysis of the self-healing ECC specimens using an environmental scanning electron microscope (ESEM) show that the crystals forming within the cracks, and on the surface adjacent to the cracks, are hydrated cement products, primarily calcium carbonate (Fig. 9). These crystal formations within the self-healed cracks are shown in Fig. 10. To facilitate healing of the cracks, and promote formation of calcium carbonate, a flow of water containing carbonates or bicarbonates must be present. Within the permeability testing, these carbonates were introduced by the constant addition of water which flows through the specimens. In the case of the partially submerged specimens, the small amount of carbon dioxide dissolved at the water surface was sufficient to cause limited self-healing at that location. However, in the absence of this constant carbonate supply, as in the saturation tanks prior to permeability testing, no self-healing of the ECC microcracks can occur. Ultimately, the formation of these crystals slows the rate of permeation through the cracked composite and further reduces the permeability coefficient.

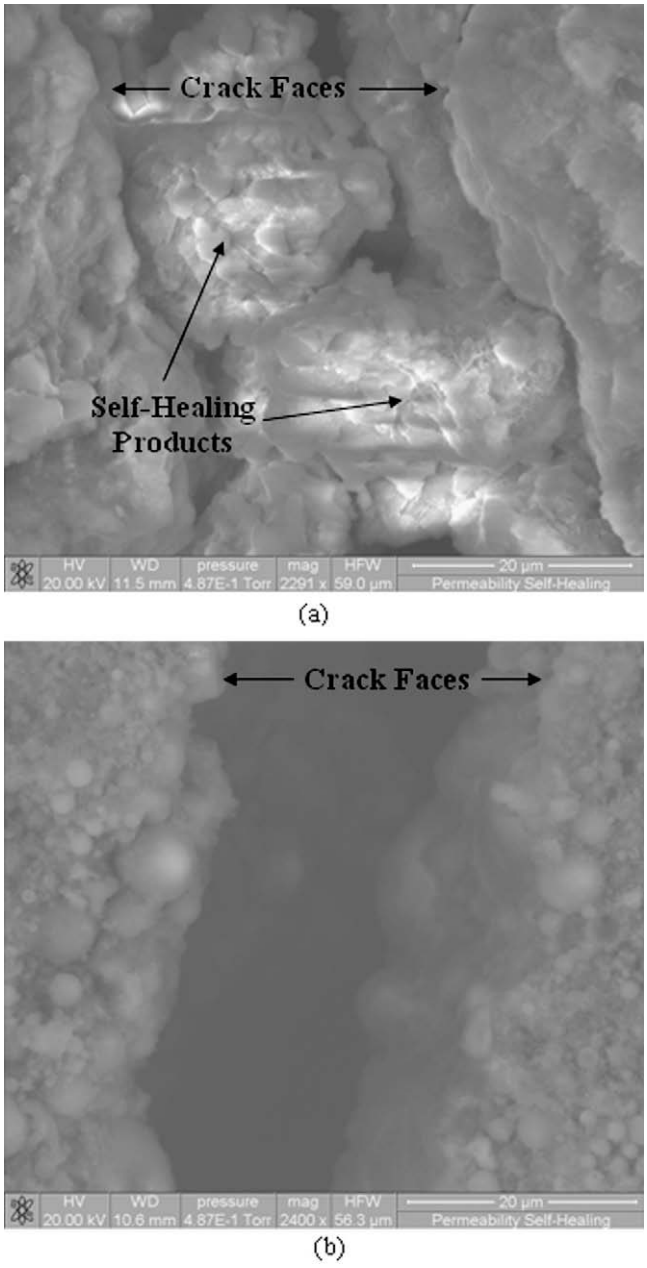

Fig. 10. (a) Autogenous self-healing crystalline formations in ECC crack after permeability testing and (b) ECC crack before permeability testing.

5. Conclusion

Within the study, the design of an ECC composite which allowed for large tensile deformations while not sacrificing a low coefficient of permeability was completed. These seemingly diametric goals were achieved by developing a composite which exhibited multiple microcracks under tension. By saturating the ECC material with microcracks of approximately 60 μm width, the unloaded permeability coefficient of the material is not compromised, and remains low even after the formation of numerous microcracks and tensile straining up to 3.0%. When compared to reinforced mortar specimens cracked under uniaxial tension to 1.5% deformation, ECC material exhibits permeability up to six orders of magnitude lower.

The tight crack widths in ECC are possible by using micromechanics as a tool for designing low permeability ECC composites which meet the two critical criteria of forming multiple cracks under load and ensuring that the maximum of the fiber bridging stress versus crack opening relationship (σ–δ) for the composite occur below a crack width opening of 100 μm. This relationship can also be used as a guide for tailoring the fiber, matrix, and fiber/matrix interface within the composite to meet the low permeability criteria. Through the use of micromechanical analysis, a version of ECC material was identified which theoretically meets the two above criteria, and was experimentally proven to exhibit low permeability in the cracked state. Additionally, through the formation of small microcracks and in the presence of water flow, a significant amount of self-healing was observed within the ECC cracks which aides in further reducing the permeability coefficient of the cracked ECC composite.

Through the use of this materials design process, in which material properties are tailored to meet a specific structural demand, the links between microstructure and structural performance are further clarified. Although this approach focused primarily on the development of a low permeability cementitious material in the cracked state for durability concerns in this paper, the application of micromechanics to tailor material properties and achieve desirable structural performance can be broadly applied within the civil engineering community.

Acknowledgements

This research was partially funded through an NSF MUSES Biocomplexity Program Grant (CMS-0223971 and CMS-0329416). MUSES (Materials Use: Science, Engineering, and Society) supports projects that study reducing adverse human impact on the total, interactive system of resource use, the design and synthesis of new materials with environmentally benign impacts on biocomplex systems, as well as maximizing the efficient use of individual materials throughout their life cycles.

References

[1] Ithuralde G. Permeability: the owner's viewpoint. In: Yves Malier, editor. High performance concrete: from material to structure; 1992. p. 276–94.

[2] Shah SP, Wang K, Weiss WJ. Is high strength concrete durable? In: Gjørv OE, Sakai K, editors. Concrete technology for a sustainable development in the 21st century; 2000. p. 102–14.
[3] Buenfeld NR. Measuring and modeling transport phenomena in concrete for life prediction of structures. In: Glanville J, Neville A, editors. Prediction of concrete durability: proceedings of STATS 21st anniversary conference; 1995. p. 77–90.
[4] Perraton D, Aitcin PC, Vezina D. Permeabilities of silica fume concrete. In: Permeability of concrete ACI SP-108. Detroit (MI): American Concrete Institute; 1988. p. 63–84.
[5] Powers TC. Structure and physical properties of hardened Portland cement paste. J Am Ceram Soc 1991;41(1):1–6.
[6] Reinhardt HW, Hearn N, Sosoro M. Transport properties of concrete. In: Reinhardt HW, editor. Penetration and permeability of concrete: RILEM report 16; 1997. p. 213–64.
[7] Lawler JS, Zampini D, Shah SP. Permeability of Cracked Hybrid Fiber-Reinforced Mortar under Load. ACI Mater J 2002;99(4):379–85.
[8] Hearn N. Effect of Shrinkage and Load-Induced Cracking on Water Permeability of Concrete. ACI Mater J 1999;96(2):234–41.
[9] Gerard B, Reinhardt HW, Breysse D. Measured transport in cracked concrete. In: Reinhardt HW, editor. Penetration and permeability of concrete: RILEM report 16; 1997. p. 265–331.
[10] Gerard B, Jacobsen S, Marchand J. Concrete cracks II: observation and permeability – a review. In: Gjorv, Sakai K, Banthia N, editors. Concrete under severe conditions 2, environment and loading, vol. 1, E&FN Spon; 1998. p. 183–97.
[11] Nowak AS, Szerszen MM. Life-cycle deterioration models for concrete deck slabs. In: Life-cycle performance of deteriorating structures, ASCE Publication; August 2003. p. 133–40.
[12] Tuuti K. Corrosion of steel in concrete. Stockholm: Swedish Cement and Concrete Research Institute; 1982.
[13] Bakker RFM. Initiation period of corrosion. In: Schiessl P, editor. RILEM report: corrosion of steel in concrete; 1988. p. 22–55.
[14] Ciampoli M (chair). Aging effects, maintenance, and structural health monitoring. In: Corotis et al., editors. Structural safety and reliability, Swets & Zeitlinger; 2001.
[15] Powers TC, Copland LE, Hayes JC, Mann HM. Permeability of Portland cement paste. ACI J Proc 1954;51(3):285–98.
[16] Mehta PK. Durability–critical issues for the future. Concr Int 1997;19(6):27–33.
[17] Wittmann FH. Crack formation and life cycle performance. In: 5th international conference on fracture mechanics of concrete structures, Vail, Colorado, USA; 2004. p. 3–10.
[18] Li VC, Stang H. Elevating FRC material ductility to infrastructure durability. In: Proceedings of 6th RILEM symposium on FRC, Varenna, Italy; 2004. p. 171–86.
[19] Wang K, Jansen D, Shah S, Karr A. Permeability study of cracked concrete. Cement Concr Res 1997;27(3):381–93.
[20] Tsukamoto M. Tightness of fiber concrete. Darmstadt Concr 1990;5:215–25.
[21] Stang H, Aarre T. Evaluation of crack width in FRC with conventional reinforcement. Cement Concr Compos 1992;14:143–54.
[22] Li VC. On engineered cementitious composites (ECC) – a review of the material and its applications. J Adv Concr Technol 2003;1(3):215–30.
[23] Weimann MB, Li VC. Drying shrinkage and crack width of ECC. Brittle matrix composites 7, Warsaw, Poland; October 2003. p 37–46.
[24] American Association of State Highway and Transportation Officials. AASHTO LFRD bridge design specifications: second edition. Washington (DC, USA): AASHTO; 1998. p. 5–41.
[25] American Concrete Institute. Building code requirements for structural concrete and commentary. Detroit (MI): ACI; 2002.
[26] Aldea CM, Shah SP, Karr A. Effect of cracking on water and chloride permeability of concrete. J Mater Civil Eng 1999(August):181–7.
[27] Rapoport J, Aldea CM, Shah SP, Ankenman B, Karr A. Permeability of cracked steel fiber-reinforced concrete. J Mater Civil Eng 2002(July/August):355–8.
[28] Marshall DB, Cox BN. A J-integral method for calculating steady-state matrix cracking stresses in composites. Mech Mater 1988(8):127–33.
[29] Li VC, Leung CKY. Theory of steady state and multiple cracking of random discontinuous fiber reinforced brittle matrix composites. ASCE J Eng Mech 1992;118(11):2246–64.
[30] Lin Z, Kanda T, Li VC. On interface property characterization and performance of fiber reinforced cementitious composites. J Concr Sci Eng, RILEM 1999;1:173–84.
[31] Wang S, Li VC. Tailoring of pre-existing flaws in ECC matrix for saturated strain hardening. In: Proceedings of FRAMCOS-5, Vail, Colorado, USA; April 2004. p. 1005–12.
[32] Li VC, Wu C, Wang S, Ogawa A, Saito T. Interface tailoring for strain-hardening PVA–ECC. ACI Mater J 2002;99(5):463–72.
[33] Redon C, Li VC, Wu C, Hoshiro H, Saito T, Ogawa A. Measuring and modifying interface properties of PVA fibers in ECC matrix. ASCE J Mater Civil Eng 2001;13(6):399–406.
[34] Cernica JN. Geotechnical engineering. New York: Holt, Reinhart & Winston; 1982 [p. 97–9].
[35] "Life-365 Service Life Prediction Model: Computer Program for Predicting the Service Life and Life-Cycle Costs of Reinforced Concrete Exposed to Chlorides" Silica Fume Association. 2001.
[36] Raupach M, Dauberschmidt C. Macrocell corrosion of reinforcement in the areas of cracks of high performance concrete. In: CONSEC '01: third international conference on concrete under severe conditions. Vancouver, BC, Canada; June 2001. p. 1506–13.
[37] Evardsen C. Water permeability and autogenous healing of cracks in concrete. ACI Mater J 1999;96(4):448–54.